Raman scattering study of interactions of cyanide impurities in KCl under variation of temperature and concentration

M. B. Grant* and M. V. Klein
Department of Physics, University of Illinois at Urbana-Champaign, 1110 West Green Street, Urbana, Illinois 68101

(Received 26 December 1984; revised manuscript received 15 April 1985)

The interactions of CN^- impurities in KCl are investigated by Raman light scattering in the spectral region of the CN^- stretching frequency. The low-temperature width and observed motional narrowing of the primary peak assigned to isolated cyanide impurities is attributed to interaction with non-near-neighbor defects in the lattice. A splitting is observed in a spectral feature attributed to CN^- pairs and attributed to a dynamical interaction (Davydov splitting). This suggests a model for nearest-neighbor pairing. The relative positions and intensities of downshifted sidebands are explained by this model.

I. INTRODUCTION

In 1977, Durand and Lüty reported a low-temperature (10 K) Raman scattering investigation of the mixed crystal $KCl_{1-x}(CN)_x$ for complete variation of the concentration ($0 \leq x \leq 1$).[1,2] They observed the evolution of this system with increasing concentration from a system of isolated $\langle 111 \rangle$ oriented CN^- rotators to a collective formation of $\langle 110 \rangle$-oriented domains. They studied two spectral neighborhoods: the region around the 2090-cm^{-1} stretching vibration of the carbon-nitrogen bond, and the low-energy region from 15 to 300 cm^{-1}. They found detailed structure in the stretching frequency region for concentrations x between 1% and 10%, which they attributed to near-neighbor collective interactions. The structure appears as multiple sidebands on the low-energy side of the main C—N stretching band. The intensities of the sidebands scale with the concentration: that of the sideband first removed from the main band was observed to scale as the square of the concentration, that of the sideband second removed as the cube of the concentration, etc.

These results motivated us to look for evidence in the Raman spectra of an order-disorder phase transition in this 1—10% range.[3–5] The ordered state would be an "orientational or elastic glass," as the defect-defect interactions are primarily paraelastic in nature. The effects of the transition should be observable by probes which are sensitive to the local strains in the crystal, as is Raman light scattering. Consequently, we have placed the stretching frequency region of the spectrum under scrutiny, with variation in concentration and temperature, seeking evidence for the onset of the disordered "freezing" of the cyanides. The evidence we expected was in the form of a rapid rate of change with the variation of temperature, of symmetry-dependent positions, widths, and strengths of spectral structures. We found no evidence of this transition, but in the attempt to do so we obtained results which lead to a model of the near-neighbor pairs responsible for some of the structure reported in the previous work. It then became clear that the spectral structure from near neighbors was a very real hindrance to tracking any structural changes resulting from long-range interactions.

We report here the observance of a minute splitting of the first sideband, i.e., that due to cyanide pairs, into two components. These we interpret as a "Davydov" doublet, i.e., an interaction-induced splitting of otherwise degenerate cyanide stretching modes into linear combinations that have even or odd symmetry under interchange of the two CN^- ions in the pair. This splitting and its temperature dependence leads us to a phenomenological picture of the near-neighbor pairing. The most plausible orientational model of the configuration of the ions in the pair provides semiquantitative agreement with experiment both for the shift of this sideband from the main band, and for the relative scattering intensity of the spectral elements attributable to isolated defects, pairs, and triplets. We attribute the width of the singlet to broadening from unresolved long-range interactions and observe its narrowing with increasing temperature (motional narrowing).

The following section describes our experimental methods. The subsequent section discusses the features and results drawn from the data along with the numerical techniques used to analyze the data. A section is then provided to describe our thinking about models of CN^- pairs and triplets. This leads us to a single pairing model which we evaluate semiquantitatively in the next section and compare with the data. A final section is provided to summarize the key conclusions and make appropriate acknowledgments.

II. EXPERIMENTAL TECHNIQUES

Three samples were obtained from the Crystal Growth Laboratory of the University of Utah. The concentrations were analyzed by M. Delong of that facility to be $(11.1 \pm 0.1)\%$, $(8.15 \pm 0.05)\%$, and $(6.05 \pm 0.15)\%$ mole fraction KCN in KCl. The Raman samples were cleaved out of the boule, leaving six orthogonal $\langle 100 \rangle$ surfaces of reasonably good optical quality. A $\langle 110 \rangle$ surface was then prepared by cutting the crystal in half along a face

diagonal with a wire saw and polishing the cut surface until it was also optically clear. The experimental configuration made available by this simple geometry has the laboratory frame oriented so that its X, Y, and Z directions correspond with the [110], [$\bar{1}$10], and [001] crystal directions, respectively. With this arrangement, the propagation direction of the incident beam coincided with the [001] axis of the crystal. The incident polarization was then either the [110] or the [$\bar{1}$10] direction. The scattered light was collected in the [$\bar{1}$10] direction with the polarization selected to be either [110] or [001]. The three polarization combinations used then were [110][110], termed $Z(XX)Y$,[$\bar{1}$10][110] or $Z(YX)Y$, and [$\bar{1}$10][001] or $Z(YZ)Y$. It can be shown from the form of the transition polarizability tensors which transform according to the Raman-allowed irreducible representations of the O_h point symmetry of the host lattice, that $Z(XX)Y$ contains a linear combination of A_{1g}, E_g, and T_{2g} scattering, $Z(YX)Y$ contains purely E_g, and $Z(YZ)Y$ contains T_{2g}. This arrangement then allows complete decomposition of the resultant spectra into the individual A_{1g}, E_g, and T_{2g} components.

A 3-l Janis Super-Vari-Temp Dewar provided the (4—300)-K temperature range that we covered in this investigation. The unit was supplied with an optical tail with four side-mounted optical windows at 90° to one another. A wire-wrapped heater on the sample block provided temperature control to within 0.1 K over the duration of a several hour run. The temperature was measured with an accuracy of within ±2 K using a gold-iron alloy—Chromel-P thermocouple on the sample block.

About 1 W of single-mode argon laser light at 5145 Å was used. The use of a Glan-Thompson prism polarizer and a double-rhomb prism-polarization rotator in the incident beam provided a beam of pure vertical polarization, at the sample area. The polarization of this beam and of the collected scattered light was automatically rotated by half-wave plates in mechanized rotators. As a result, at each monochromator setting, all three of the polarization combinations were obtained essentially simultaneously, thus ensuring equivalent normalization and accurate relative positions of spectral structures. It was then assumed that point-by-point linear combinations of the spectra would successfully separate out the scattering due to each allowed symmetry. The collection optics consisted of a Canon $f/1.5$, 85-mm lens. This lens collimated the scattered light into an $f/8$ achromatic doublet of about 400 mm focal length. The doublet then focused the scattered light onto the vertical entrance slit of the monochromator. The laser-beam waist in the sample was horizontal. Image rotation through 90° was achieved by three 45° mirrors.

The monochromator used was a Spex model 1401 double, fitted with 0.85-m focal length mirrors (approximately $f/8$ entrance aperture) and holographic gratings having 1800 grooves/mm. The detector was an RCA C31034 photomultiplier tube used with photon-counting electronics. The reciprocal dispersion of the instrument was 100 μm per wave number in the green. The desired high resolution required that the monochromator be operated near the diffraction limit. To achieve this we found that the waist of the laser beam as it was focused in the sample must be centered on the optical axes of the collection optics and that the collection optical axis must coincide with the entrance optical axis of the monochromator. This was accomplished by a procedure similar to that used to align the optics associated with a Fabry-Perot interferometer. Once the collection optics were precisely positioned along the entrance optical axis, they were then considered as part of the optical system of the monochromator and remained untouched throughout the data-gathering process. With this procedure and with the slits opened to 20 μm, we obtained an instrument function of 0.3 cm^{-1} full width at half maximum (FWHM), which did not degrade in peak intensity or shape over the course of several runs.

The pass-function width and shape were verified by using the monochromator to obtain the spectrum of a neon lamp in the spectral vicinity of the desired Raman-scattered light. There is a relatively intense line in the spectrum of singly ionized, excited neon which occurs at 17 248 cm^{-1}. This is close to the Stokes Raman scattering line of CN^- in KCl when excited by the 5145-Å (19 435-cm^{-1}) argon line. This neon line was also used to calibrate the monochromator drive, since the spectral region being explored is relatively far removed from the frequency of the incident laser light. This procedure was not used between successive runs for the sake of efficiency, but was used before, during, and after an entire set of 10—20 runs. We estimate that the reported absolute positions of spectral features are accurate to within $\pm\frac{1}{2}$ cm^{-1}. Relative positions of features in the same run could generally be measured better than an order of magnitude more precisely than that, due to the assistance of numerical analysis and the automatic symmetry separation. If shifts in the position of this neon line were observed, then a linear correction was made to the positions of the $KCl_{1-x}(CN^-)_x$ spectra according to the time that the data were taken versus the time at which the neon lines were evaluated.

III. EXPERIMENTAL RESULTS

Figures 1 through 6 show representative spectra obtained for the three different samples. For each concentration, the three spectra corresponding to the three Raman-allowed modes are shown for both low temperature (12 to 14 K) and intermediate temperature (60 to 61 K). For the 6% sample, the peak at 2088 cm^{-1} is the main band. This peak occurs at 2088 and 2087 cm^{-1} at low and intermediate temperatures, respectively, for the 8% sample and at 2087.5 and 2087 cm^{-1} for the 11% sample. The main band results from isolated cyanide impurities (having no near-neighbor cyanide ions). The first sideband, attributed here to the response of cyanide pairs, is the major peak that occurs about 1 cm^{-1} lower than the main band in all cases. The second sideband is the broad and relatively weak structure in the lower-frequency wing about 4 to 5 cm^{-1} below the main band. This is the spectral component that is believed to be the response of CN^- triplets.

The separation of the different representations was accomplished by point-by-point subtraction of one-third of

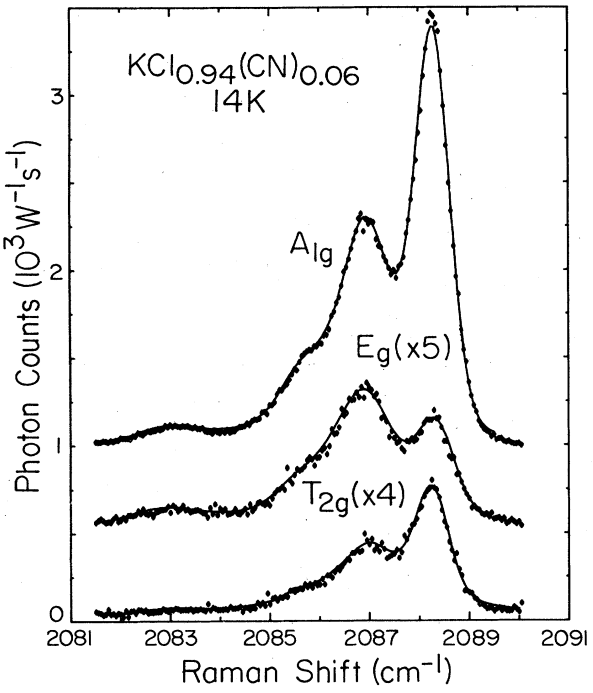

FIG. 1. A_{1g}, E_g, and T_{2g} spectra of the $KCl_{1-x}(CN^-)_x$ sample for $x=0.06$ at $T=14$ K. For visual clarity, the curves have been shifted vertically and the E_g and T_{2g} spectra have been multiplied point-by-point by the indicated factors. The solid lines through the actual data points are representative of least-squares computer fits.

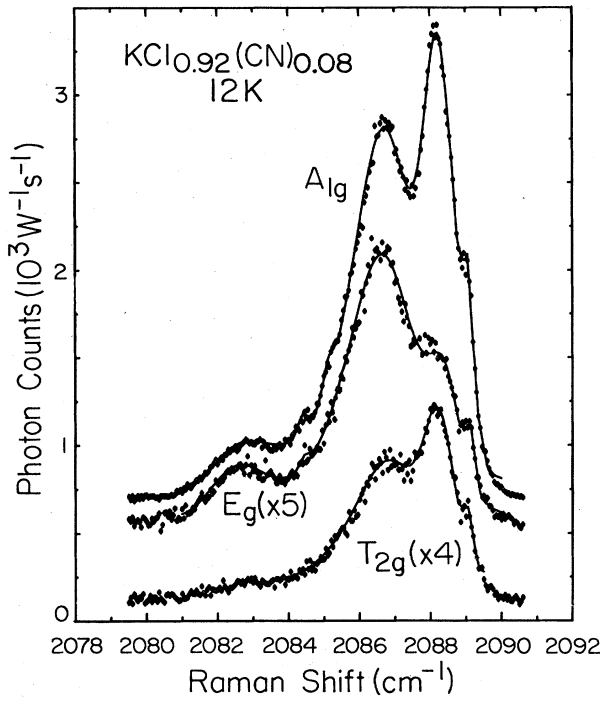

FIG. 3. A_{1g}, E_g, and T_{2g} spectra for $x=0.08$ at $T=12$ K.

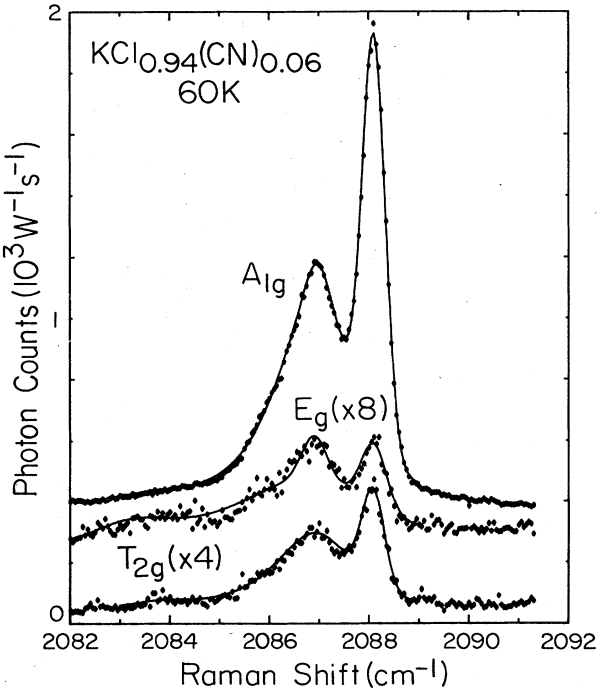

FIG. 2. A_{1g}, E_g, and T_{2g} spectra for $x=0.06$ at $T=60$ K.

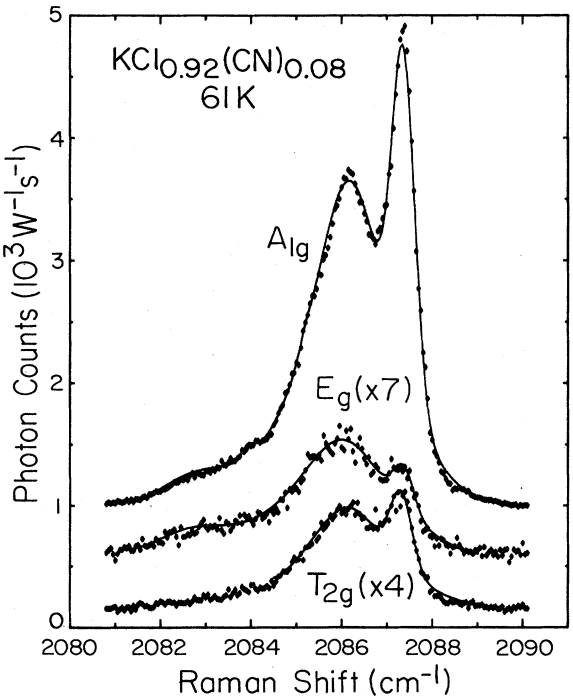

FIG. 4. A_{1g}, E_g, and T_{2g} spectra for $x=0.08$ at $T=61$ K.

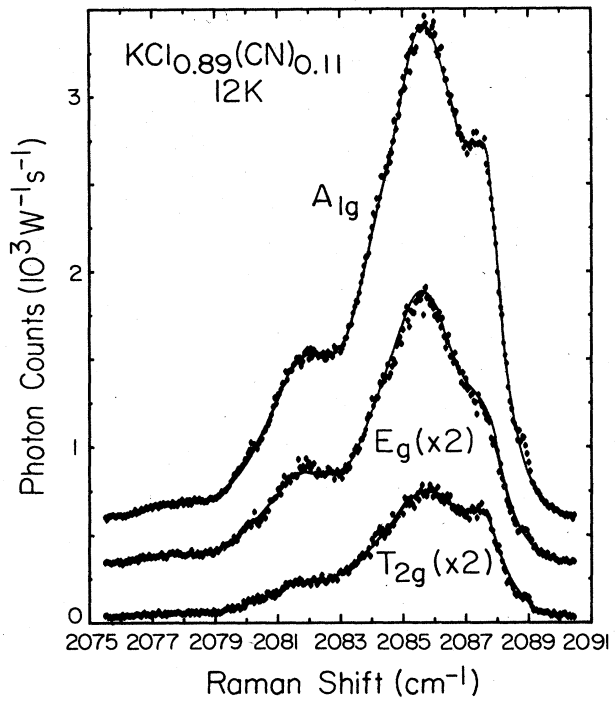

FIG. 5. A_{1g}, E_g, and T_{2g} spectra for $x=0.11$ at $T=12$ K.

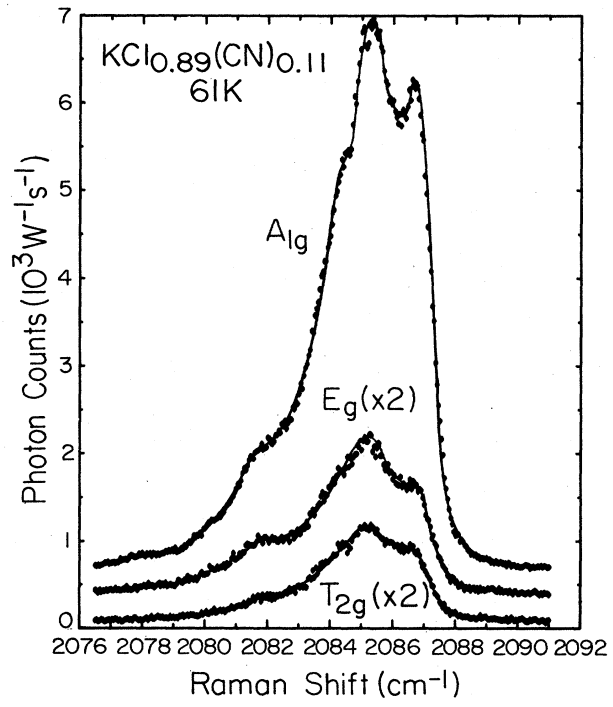

FIG. 6. A_{1g}, E_g, and T_{2g} spectra for $x=0.11$ at $T=61$ K.

the $Z(YX)Y$ spectrum and the entire $Z(XZ)Y$ polarization spectrum from the $Z(XX)Y$ spectrum. The resultant data file was then labeled A_{1g}, whereas $\frac{4}{3}$ of the $Z(YX)Y$ spectrum and the $Z(YZ)Y$ spectrum were labeled E_g and T_{2g}, respectively. The convention used here for the normalization coefficients of the polarizability tensors, that of Hayes and Louden,[6] indicates that the $Z(XX)Y$ and $Z(YZ)Y$ spectra containing the entire T_{2g} scattering strength, whereas the convention used by Durand and Lüty,[2] for example, indicates these scattering geometries both contain half the full T_{2g} component. The reliability of this procedure was ensured by the use of the automatic polarization rotators mentioned earlier.

The solid lines through the data points are calculated from least-squares fits which were performed to determine peak positions, widths, and intensities. In all cases, the main band was assumed to be inhomogeneously broadened and, therefore, Gaussian in shape. The sidebands were fit by Lorentzians convoluted into the Gaussian of the main band. The sidebands thus appear to be homogeneously broadened, due presumably to relatively rapid decay of the excited vibrational state. In fitting the data we convoluted the instrument function into model line shapes for all of these structures, and the Gaussian structure of the main band was convoluted into the model line shapes of the sidebands. The latter was done because it was assumed that the broadening that the isolated defects undergo due to long-range interactions would also be experienced by the defect pairs and triplets. Residual bands which occurred above the main band and between the more substantial sidebands have for the most part remained unresolved and unassigned. We did fit line shapes to them, in order to report the positions, widths, and intensities of the primary structures as accurately as possible. These residual bands were fitted with structures of equal width and shape as the main band, and their intensities were allowed to vary for computer optimization. We speculate about their origins later in this paper.

Upon casual inspection it is seen that these spectra cannot be due to Raman-allowed transitions between energy levels of the hindered CN^- rotor. No structure was observed above the main band at low temperature, but rather all observed structure occurs below the main band no matter what the temperature. Durand and Lüty[1,2] have shown that the intrinsic Raman features of the isolated CN^- stretching band are only observed in samples of "negligible" concentration ($x \leq 0.05$). Their spectra are quite different from those in Figs. 1—6, leading one to the conclusion that the structure we observe is attributable to interactions among defects.

We first discuss the spectral features of the A_{1g} spectra. The most notable characteristic is the narrowing of the main band with *increasing* temperature for all three samples. This is a continuous effect, as seen in Fig. 7. At the lowest temperatures, the widths from 6%, 8%, and 11% samples are approximately 0.85, 1.0, and 1.1 cm^{-1}, respectively. These widths first decrease rapidly with increasing temperatures until they reach minima near 100 K. The minima are approximately 0.42 cm^{-1} for $x=0.11$, 0.38 cm^{-1} for $x=0.08$, and 0.33 cm^{-1} for $x=0.06$. This remaining width at 100 K is believed to be

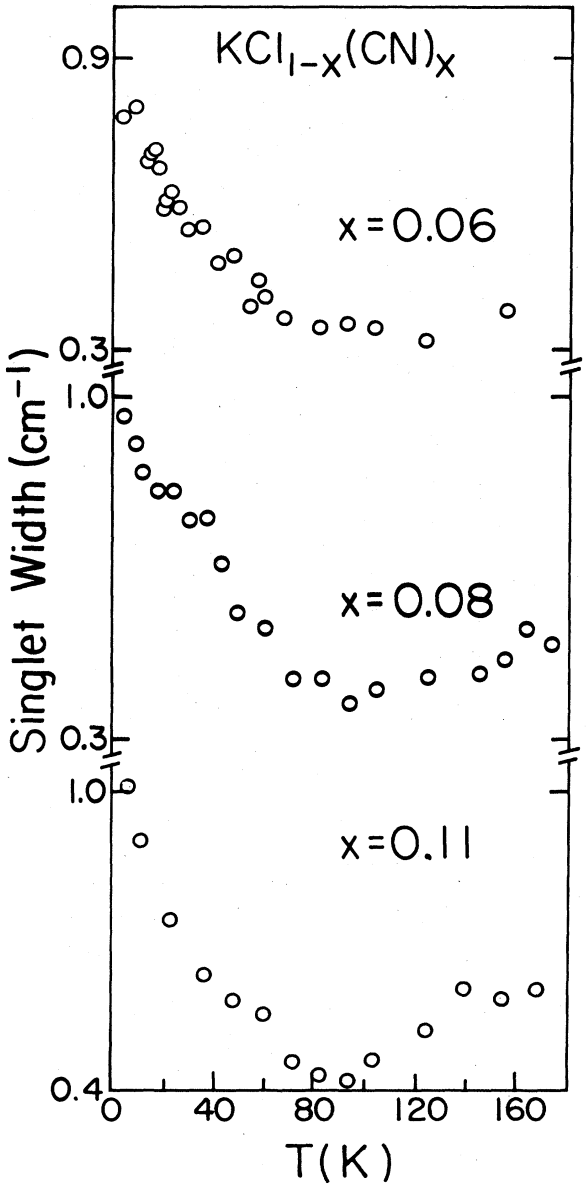

FIG. 7. Variation with temperature of the full width at half maximum (FWHM) of the main band or singlet peak in the A_{1g} spectra for CN^- concentrations (x) of 0.06, 0.08, and 0.11.

true spectral broadening since our convolution procedure has removed the instrumental width and since the peak still appears to be Gaussian. This residual width is probably due to interactions with distant CN^- impurities, as will be discussed later. Above 100 K the width of the main band in all three concentrations begins to increase. At room temperature for $x=0.06$ and 0.08 the remaining structure appears as two overlapping peaks which are unresolved from one another. The A_{1g} spectrum from the $x=0.11$ sample appears more like a single peak at 295 K. Assuming that the spectra from all three samples are composed of two peaks, we obtained a room temperature width of 0.8 to 0.9 cm^{-1} for the main band in every case. The uncertainty here is due to the difficulty in obtaining a unique pair of peaks that constitute this unresolved structure. The total width of the double peak was 1.7 cm^{-1} for all three concentrations.

Figures 8—10 show the shifts in the peak positions of the main band and the first and second sidebands with temperature, obtained from the numerical fits to the A_{1g} spectra for the three concentrations. The main bands are within $\pm\frac{1}{2}$ cm^{-1} of each other below 10 K for the three concentrations. Table I lists the values obtained. The resulting positions tend to agree with the previous results of Callender and Pershan[7] and Lüty *et al.*[1,2,8]

For all three samples, the first sideband tends to track with the main band along with a small degree of narrowing of the difference between their positions with increasing temperature. In the 6% sample, the difference between the two positions tends to about 1.4 cm^{-1}, about 1.6 cm^{-1} for 8%, and about 2.0 cm^{-1} for the 11% case (Table I). For the 6% sample (Fig. 8), however, the curves all tend to have a more positive slope. An uncompensated systematic error may be the cause. It could be attributed to a nonlinear drift in the monochromator drive with time, which our calibration procedure failed to correct.

The second sidebands appear to show little softening with increasing temperature. All three tend to blend into the remaining broad double-peaked structure that remains at room temperature. For the 11% sample (Fig. 10) we were only able to resolve the band up to about 60 K. Separation of the second sideband from the main band for

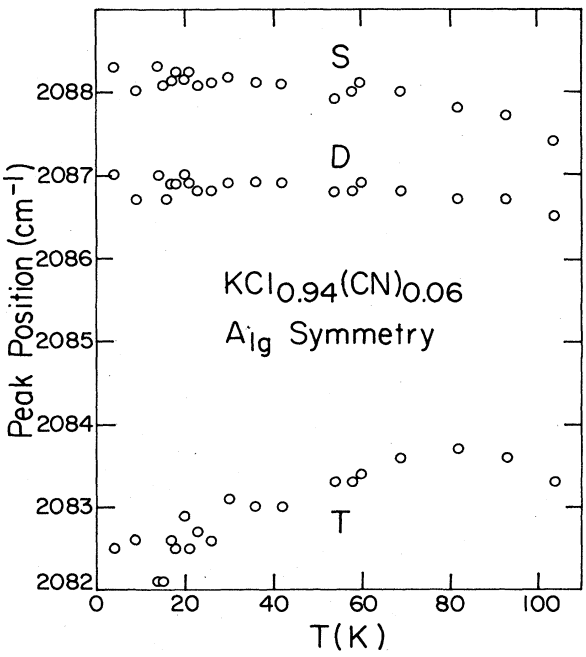

FIG. 8. The positions vs temperature in the A_{1g} spectra of the main band (S), the first sideband (D), and the second sideband (T) for a CN^- concentration (x) of 0.06.

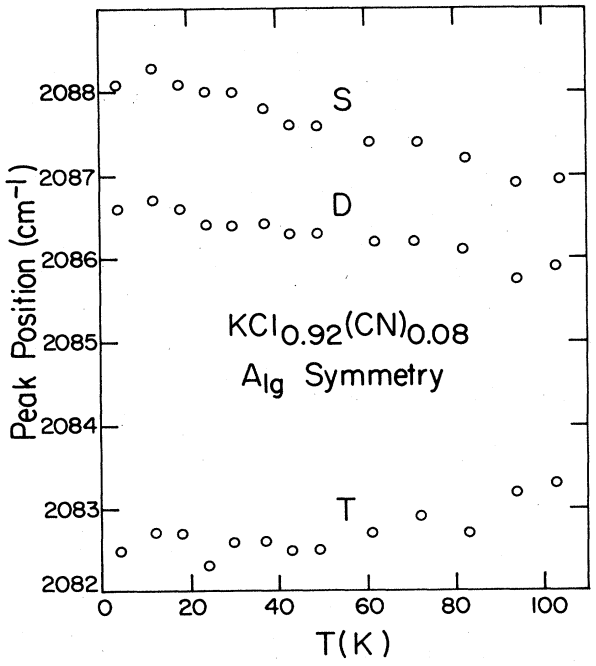

FIG. 9. The positions vs temperature in the A_{1g} spectra of the main band (S), the first sideband (D), and the second sideband (T) for a CN^- concentration (x) of 0.08.

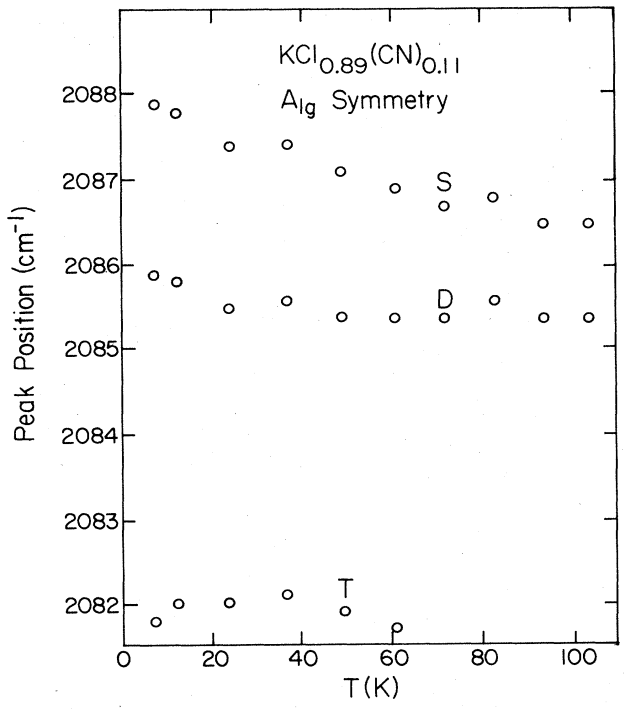

FIG. 10. The positions vs temperature in the A_{1g} spectra of the main band (S), the first sideband (D), and the second sideband (T) for a CN^- concentration (x) of 0.11.

TABLE I. Absolute position, separation, and slopes of the main band and first sideband in the A_{1g} spectra.

Parameter	CN^- concentration (x) 0.06	0.08	0.11
Low-temperature Main-band position (cm^{-1})	2088.7	2088.3	2087.9
Low-temperature first-sideband position (cm^{-1})	2087.3	2086.7	2085.9
Separation between main band and first sideband (cm^{-1})	1.4	1.6	2.0
Linear slope ($\Delta\omega/\Delta T$) of main band (10^{-2} cm^{-1}/K)	−1.22	−1.41	−1.31
Linear slope ($\Delta\omega/\Delta T$) of first sideband (10^{-2} cm^{-1}/K)	−0.81	−0.84	−0.56

all three concentrations was consistently about 6 cm^{-1} at low temperature (Table I).

The relative intensities of the first and second sidebands in the A_{1g} spectra should indicate the concentration dependence of the features. The observed ratio of the integrated intensity of a sideband to that of its main band in any sample does not seem to vary significantly with temperature, as long as the sideband can be resolved. This ratio for the first sideband was 0.97 ± 0.04, 1.44 ± 0.09, and 2.09 ± 0.07 for $x=0.06$, 0.08, and 0.11, respectively, for temperatures up to about 60 K. For the second sideband it was 0.094 ± 0.07, 0.19 ± 0.02, and 0.40 ± 0.02 in the same order. We will discuss the significance of these numbers in a following section.

At temperatures less than 60 K, the A_{1g} structures appear somewhat asymmetric, but this is only an artifact of the unresolved residual bands on their low-energy side. Yet as 100 K is approached, all these features become heavily skewed toward the lower frequencies. This effect is markedly greater for the higher-concentration samples. Towards 100 K and above it causes difficulty in fitting with symmetric functions.

Thus far, the discussion has centered on the features contained in the A_{1g} spectra. Upon inspection of the E_g and T_{2g} spectra in comparison to the A_{1g}, in Figs. 1—6, it can be seen that the E_g spectra have significantly less relative intensity in the main band compared to the first sideband for all three concentrations. The relative intensities of T_{2g} spectra appear more like those of A_{1g} symmetry. In fact, the remaining intensity in this E_g main band is about 2% of the intensity of the corresponding structure in the A_{1g} spectra, whereas it is 6—10% in the T_{2g} symmetry. This 2% is precisely the expected amount of leakage of polarized (A_{1g}) scattering into unpolarized spectra due to the finite-collection solid angle of our $f/1.5$ collection optics. We therefore conclude that this peak in the E_g spectra is due solely to leakage and that there is no

intrinsic scattering of E_g symmetry of the CN^- molecules that are isolated in the host lattice (i.e., having no near-neighbor cyanides).

The final and most notable observation we extract from the data concerns the relative positions of the first sideband in the A_{1g}, E_g, and T_{2g} spectra for the three samples. For low temperatures (Figs. 1, 3, and 5), one can see that the peak of the T_{2g} first sideband is upshifted from that in the A_{1g} and E_g spectra by what appears to be about $\frac{1}{4}$ cm^{-1}. The careful fits of these data resulted in the plots shown in Fig. 11. We find the T_{2g} mode to be 0.09 ± 0.02 cm^{-1} above the average of the E_g and A_{1g} modes for the 6% sample, 0.14 ± 0.02 cm^{-1} for 8%, and 0.14 ± 0.04 cm^{-1} for 11%. Above 40 K the splitting abruptly decreases and is gone by 50 K. This lack of splitting at the higher temperatures can be observed by eye as well in Figs. 2, 4, and 6 at around 60 K. We believe this splitting to be well-established. It agrees at least in magnitude with a simple model of CN^- pairs which we will now describe.

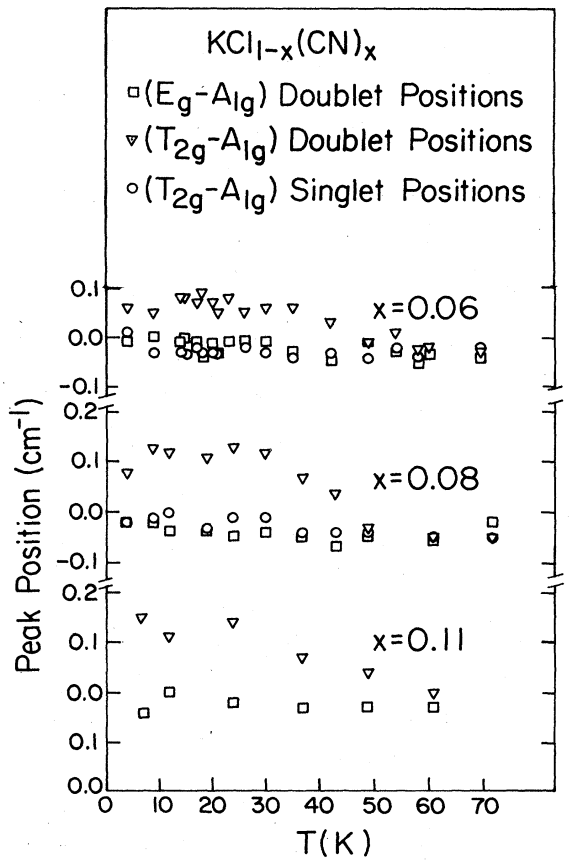

FIG. 11. Difference between the positions of the first sideband in the T_{2g} and A_{1g} spectra (▽), and in the E_g and A_{1g} spectra (□), and the positions of the main band in the T_{2g} and A_{1g} spectra (○) for the three concentrations. The E_g-to-A_{1g} first-sideband (doublet) separation and the T_{2g}-to-A_{1g} main-band (singlet) separation are included to emphasize the splitting between the T_{2g} and A_{1g} first-sideband positions.

IV. CYANIDE PAIR AND TRIPLET MODELS

In order to analyze these data, we now determine the effect of other cyanide impurities at the site of a given CN^- ion. Atomic displacements, impurity interactions, and pair-excitation modes must be determined in order to verify quantitatively that the observed downshifts and splittings of the stretching vibration are results of near-neighbor interactions. For this reason, we develop a microscopic model of a cyanide pair with its interaction and vibrational modes. First, the interaction energy will be discussed and then orientational models that minimize this energy will be identified.

Lüty and Beyeler[8,9] have fully studied the isolated CN^- impurity in KCl and have confirmed the elongated defect as having orientational potential minima in the $\langle 111 \rangle$ crystal directions. For $KCl_{1-x}(CN)_x$ with $x > 0.80$, the CN^- molecules align along $\langle 110 \rangle$ face diagonals at lower temperatures.[1,2,10] It is not initially obvious as to which of these alignments is assumed by the near-neighbor impurity pairs. We recall that we observed no intensity in the E_g spectra from the single band, apart from leakage. This corroborates the $\langle 111 \rangle$ model for the isolated impurity since one can show that the $\langle 111 \rangle$ model with its C_{3v} symmetry does not contribute an E_g component to the stretching band.

The CN^- molecule displaces more volume in KCl than does the Cl^- ion it replaces. From x-ray measurements it is known that the radius of Cl^- in KCl is 1.81 Å. The semiminor axis of the CN^- ellipsoid has a length of 1.78 Å, while the semimajor axis is 2.15 Å long. Thus the cyanide impurity displaces 28.5 $Å^3$ in the lattice compared to 24.8 $Å^3$ for the chlorine ion.[11–13] When a CN^- defect is substituted for a Cl^- ion in KCl, the cyanide stretching frequency increases above its value in the gaseous state due to the compression that the anharmonic C—N bond experiences in the lattice. If two CN^- molecules exist as near neighbors to one another and their major interaction is that of strain, then the lower-energy configuration is one of lowest strain, such that the strain around each CN^- in the pair is less than that of an isolated CN^-. If the bonds are less strained, the stretching frequencies will be lower. On an atomic scale this effect will occur if each CN^- ion in the pair were to assist the other in pushing out on the host lattice ions. The models we consider must accommodate this criterion.

We should also consider the electric dipole interaction. The CN^- ion in KCl has been shown to have a static dipole moment of 0.3 to 0.4 D or 0.06 to 0.08 e Å.[9,14,15] This is understandably small compared with other diatomic molecular ions in which the bond is more fully ionic in nature. In the dielectric studies of Julian and Lüty[16] it was shown for the phase transition at 168 K in KCN that although there is hysteresis and domain formation there is no observed dielectric loss. Yet for the 83-K transition, a definite dielectric loss was found. They conclude that the upper transition is "ferroelastic" in nature with the CN^- head and tail still free to reorient, and that the lower transition is that of antiparallel ordering of the electric dipole moments. This implies that the electric-dipole—dipole interaction is significantly weaker than the

elastic interactions. We nevertheless include this effect by use of the phenomenological interaction

$$W_{12}=\frac{1}{\epsilon}\left[\frac{\mathbf{P}_1\cdot\mathbf{P}_2}{r^3}-3\frac{(\hat{\eta}_{12}\cdot\mathbf{P}_1)(\hat{\eta}\cdot\mathbf{P}_2)}{r^3}\right] \quad (1)$$

to find the pair energies for the different possible orientations. In this expression ϵ is taken to be the dielectric constant of the host KCl crystal, and $\mathbf{P}_1$ and $\mathbf{P}_2$ are the static CN^- dipole moments. The unit vector $\hat{\eta}_{12}$ and distance r are given by the expressions

$$\hat{\eta}_{12}=\frac{(\mathbf{r}_1-\mathbf{r}_2)}{|\mathbf{r}_1-\mathbf{r}_2|},\quad r=|\mathbf{r}_1-\mathbf{r}_2|\ ,$$

where $\mathbf{r}_1$ and $\mathbf{r}_2$ are position vectors for the two dipoles relative to an arbitrary origin. For nearest-neighbor anion sites in the NaCl structure, the separation r is fixed at $\sqrt{2}a$, and to first order we can assume that the magnitudes of the dipole moments are independent of orientation. Thus comparing the above energies for different orientations reduces to evaluating the term

$$\frac{W_{12}}{W_0}=[\hat{\mathbf{P}}_1\cdot\hat{\mathbf{P}}_2-3(\hat{\eta}_{12}\cdot\hat{\mathbf{P}}_1)(\hat{\eta}_{12}\cdot\hat{\mathbf{P}}_2)]\ , \quad (2)$$

where

$$W_0=\frac{P^2}{\epsilon(\sqrt{2}a)^3}\ .$$

The electrical and strain interactions also have another contribution, of a dynamic nature. The T_{2g} to A_{1g} splitting of the first sideband is most likely a Davydov type of splitting due to coupled stretching vibrations of the two individual cyanides comprising the near-neighbor pair. Such splitting will occur only if the two cyanides in the pair are equivalent. The 2100-cm^{-1} frequency is too high for the coupling to involve the displacement of lattice ions. Therefore this coupling is probably due either to the electric dipole interaction or the direct repulsive interaction between the electron shells of the CN^- molecular ions themselves. These interactions are decoupled from the lattice to first order. The magnitude of the coupling is directly related to the measured splitting so that this consideration also provides a check of the correctness of pair-configuration models.

We now consider the possible alignment models to find the optimum ones. Some general considerations will avoid the detailed evaluation of every case. Obviously, if both molecules are aligned along the [110] direction separating them, even though this can be a situation in which the energy of the electrical interaction is minimized, it is one in which the stress is maximized. If one defect points directly at the waist of the other so that the two major axes are perpendicular, then to first order there is no mutual reduction in elastic energy, and the electric dipole energy is zero. There will be, in addition, no Davydov splitting since the sites are inequivalent. One other unlikely alignment is that in which the two major axes of the impurities lie in or nearly in planes that are perpendicular to the [110] direction separating them and in which the two major axes are skewed relative to one another. This configuration also gives electric dipole or repulsive energies that are very nearly zero for static alignment or dynamic coupling, and it offers little mutual reduction in the stress on each molecule since their directions of elongation are also outward, toward pure areas of the lattice.

The remaining cases to be considered are those in which the defects are parallel and at the same time perpendicular to the [110] direction between them or those in which they "nod" toward each other. Figure 12 depicts the four such cases: two where the CN^- alignment is ⟨110⟩ and two where it is ⟨111⟩. Each type of alignment has one case in which the cyanides are *parallel* to each other while perpendicular to the [110] direction that separates them, and one case in which the molecules are "*nodding*" toward each other.

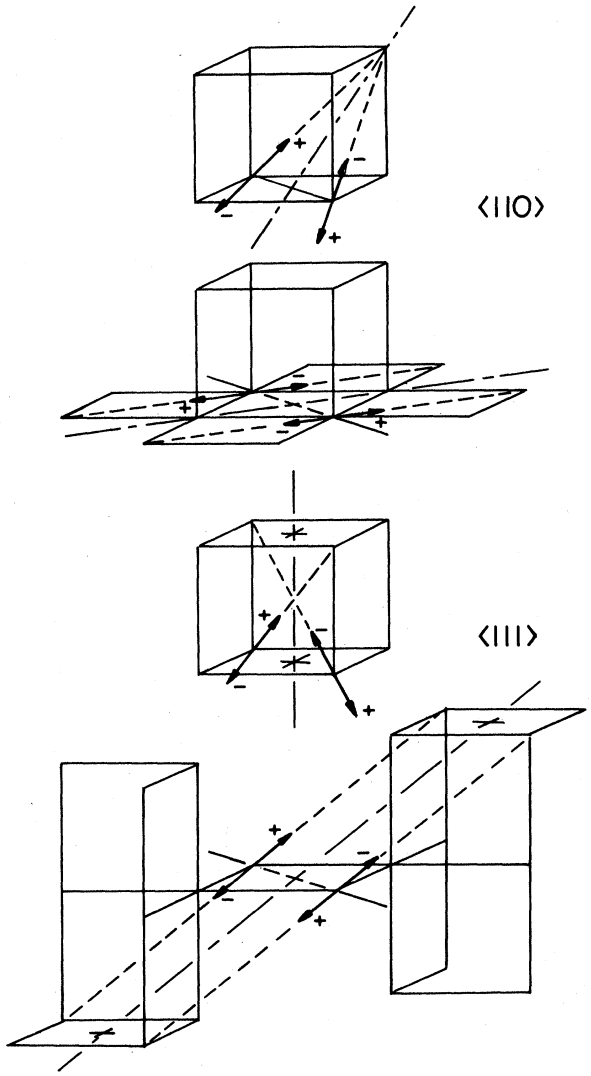

FIG. 12. The different possible configurations of CN^- pairs which minimize the strain and electric dipole interactions. From top to bottom, alignment of the cyanides in the ⟨110⟩ direction is shown for the "nodding" and "parallel" cases, respectively. Then ⟨111⟩ alignment is shown for the "nodding" and "parallel" cases, respectively. The pair-site symmetries indicated are those of the pairs only with no regard for their electric dipole moment shown or the host crystal.

If the observed T_{2g} and A_{1g} splitting (see Fig. 11) is a Davydov-type splitting, then one symmetry operation of the crystal must take one of the cyanides into the other. Then the stretching vibrations are coupled, and the resultant peak is split between the modes that are odd or even under this operation. This is precisely what we observe, as seen in Fig. 11. This situation is true for all four of these models in Fig. 12. In each case there is a reflection plane of the lattice which is also a reflection plane of the pair, if we can ignore the electric dipole alignment as causing negligible difference between the two oscillators in the pair. The ⟨110⟩ *parallel* and ⟨111⟩ "*nodding*" alignments also have a common twofold rotation axis with the lattice that takes one defect in the pair into the other. For both the ⟨110⟩ and ⟨111⟩ *parallel* configurations, the pair symmetry is D_{2h} (mmm), which has full inversion symmetry. Odd-parity irreducible representations will then be Raman inactive. This implies that the odd member of the Davydov doublet will be Raman inactive, contrary to our results.

The remaining models are the two "*nodding*" cases which we will now evaluate. These configurations provide strong mutual local stress reduction by simultaneously pushing out on shared neighbor ions. In the ⟨110⟩ case, both of the CN^- impurities push out on the two Cl^- ions along the symmetry axis between them. For the ⟨111⟩ alignment, each of the two K^+ ions at the narrow end of the pair is displaced by both cyanides. These cases have the lowest possible electrostatic interactive energies. The square-bracketed term on the right-hand side of Eq. (2) is $-\frac{5}{3}$ and $-\frac{5}{4}$ for the ⟨111⟩ and ⟨110⟩ configurations, respectively. These cases also provide significant electric dipole interaction terms for coupled stretching vibrations. The repulsive interaction is substantial between the electron shells on the ends of the CN^- ions that are brought near to each other, resulting in stronger coupling as well.

Before we do a quantitative analysis, we will here ensure that symmetry arguments based on these "nodding" models do agree with the observed results. The two modes of the coupled defects are the symmetric mode in which the two CN^- ions stretch in phase and the antisymmetric mode in which they oscillate out of phase. The correlation of the irreducible representations corresponding to these modes in these two "nodding" configurations and those of O_h can be shown by writing the dynamical polarizabilities for stretching vibrations as

$$\begin{aligned}\delta\vec{\vec{\alpha}}_1&=\delta\vec{\vec{\alpha}}I+a\hat{\mathbf{n}}_{11}\hat{\mathbf{n}}_{11}+b\hat{\mathbf{n}}_{12}\hat{\mathbf{n}}_{12}+c\hat{\mathbf{n}}_{12}\hat{\mathbf{n}}_{13}\,,\\ \delta\vec{\vec{\alpha}}_2&=\delta\vec{\vec{\alpha}}I+a\hat{\mathbf{n}}_{21}\hat{\mathbf{n}}_{21}+b\hat{\mathbf{n}}_{22}\hat{\mathbf{n}}_{22}+c\hat{\mathbf{n}}_{23}\hat{\mathbf{n}}_{23}\,,\end{aligned}\tag{3}$$

where $\hat{\mathbf{n}}_{ij}$ is the jth symmetry axis of the ith defect. The dyad $\hat{\mathbf{n}}_{ij}\hat{\mathbf{n}}_{ij}$ obeys the relation

$$(n_{ij}n_{ij})_{\alpha\beta}=n_{ij\alpha}n_{ij\beta}\,.$$

Now, for the ⟨111⟩ model [Fig. 13(a)],

$$\begin{aligned}&\hat{\mathbf{n}}_{11}=\frac{1}{\sqrt{6}}[11\bar{2}],\quad \hat{\mathbf{n}}_{12}=\frac{1}{\sqrt{2}}[1\bar{1}0],\quad \hat{\mathbf{n}}_{13}=\frac{1}{\sqrt{3}}[111]\,,\\ &\hat{\mathbf{n}}_{21}=\frac{1}{\sqrt{6}}[112],\quad \hat{\mathbf{n}}_{22}=\frac{1}{\sqrt{2}}[\bar{1}10],\quad \hat{\mathbf{n}}_{23}=\frac{1}{\sqrt{3}}[\bar{1}\,\bar{1}1]\,.\end{aligned}\tag{4}$$

The dynamical polarizability of the symmetric mode is given by

$$\delta\vec{\vec{\alpha}}_1+\delta\vec{\vec{\alpha}}_2=2\left[\delta\alpha+\frac{a+b+c}{3}\right]\vec{\vec{1}}+\begin{bmatrix}\frac{-(a-b)}{3} & \frac{(a-3b+2c)}{3} & 0\\ \frac{(a-3b+2c)}{3} & \frac{-(a-b)}{3} & 0\\ 0 & 0 & \frac{2(a-b)}{3}\end{bmatrix},\tag{5}$$

and that of the antisymmetric mode is

$$\delta\vec{\vec{\alpha}}_1-\delta\vec{\vec{\alpha}}_2=\begin{bmatrix}0 & 0 & \frac{2(c-a)}{3}\\ 0 & 0 & \frac{2(c-a)}{3}\\ \frac{2(c-a)}{3} & \frac{2(c-a)}{3} & 0\end{bmatrix}.\tag{6}$$

In the O_h point group of the host lattice, the terms in Eqs. (5) and (6) that are proportional to the identity matrix, transform like the A_{1g} irreducible representation, while the off-diagonal terms transform like T_{2g} and the traceless diagonal parts transform like E_g. The polarizability in the antisymmetric mode in Eq. (6) transforms totally like T_{2g}. Since we see the T_{2g} component of the first sideband upshifted from the other components, the symmetric mode must have little T_{2g} character. We can therefore conclude that

$$(a-3b+2c)\simeq 0\,.\tag{7}$$

Due to the shape of the defect, namely, elongated in the z direction, we can say that $c>a,b$. If we then assume that $a=c-\delta$, $b=c-\epsilon$, then Eq. (7) implies that $\epsilon=\delta/3$. If we assume $\delta=0.3$, then $b/c=0.9$ and $a/c=0.7$. These values are not unreasonable, considering the geometry of the defect discussed earlier in this section. The result is that we have the symmetric mode only in A_{1g} and E_g symmetry and the antisymmetric mode only in T_{2g} symmetry, as our data suggest.

For the ⟨110⟩ model [Fig. 12(a)],

$$\begin{aligned}&\hat{\mathbf{n}}_{11}=\frac{1}{\sqrt{2}}[1\bar{1}0],\quad \hat{\mathbf{n}}_{12}=[001],\quad \hat{\mathbf{n}}_{13}=\frac{1}{\sqrt{3}}[110]\,,\\ &\hat{\mathbf{n}}_{21}=\frac{1}{\sqrt{2}}[\bar{1}0\bar{1}],\quad \hat{\mathbf{n}}_{22}=[0\bar{1}0],\quad \hat{\mathbf{n}}_{23}=[\bar{1}01]\,.\end{aligned}\tag{8}$$

This provides a symmetric mode with

$$\delta\vec{\vec{\alpha}}_1+\delta\vec{\vec{\alpha}}_2=2\left[\delta\alpha+\frac{a+b+c}{3}\right]\vec{\vec{I}}+\begin{bmatrix}\frac{(a-2b+c)}{3} & \frac{-(a-c)}{2} & \frac{(a-c)}{2}\\ \frac{-(a-c)}{2} & \frac{-(a-2b+c)}{6} & 0\\ \frac{(a-c)}{2} & 0 & \frac{-(a-2b+c)}{6}\end{bmatrix} \tag{9}$$

and an antisymmetric mode with

$$\delta\vec{\vec{\alpha}}_1-\delta\vec{\vec{\alpha}}_2=\begin{bmatrix}0 & \frac{-(a-c)}{2} & \frac{-(a-c)}{2}\\ \frac{-(a-c)}{2} & \frac{(a-2b+c)}{2} & 0\\ \frac{-(a-c)}{2} & 0 & \frac{-(a-2b+c)}{2}\end{bmatrix}. \tag{10}$$

In this case, the symmetric mode has all three Raman-active representations (A_{1g}, E_g, and T_{2g}), and the antisymmetric mode has both E_g and T_{2g} terms. We do not observe the antisymmetric E_g or the symmetric T_{2g} components in our data, yet if we try to set these coefficients to zero in the above model, then the T_{2g} antisymmetric and E_g symmetric modes, which we do see in our data, also become zero since the coefficients of these components are identical in both. This argues for the $\langle 111\rangle$ picture at this point, if the primary assumption is correct that the two CN^- ions experience the same environment.

V. QUANTITATIVE ANALYSIS OF THE MODEL

To answer this last question and to examine our model's quantitative validity, we need to estimate the strain and electric-dipole–dipole interactions. We will obtain semiquantitative values for the first sideband splitting, the relative sideband intensities, the symmetry splitting of the first sideband, and the motional narrowing to be compared to the measured values.

A. First sideband splitting

We observe an overall drop of the stretching frequency when two impurities find themselves as near neighbors to each other. As pointed out at the beginning of the preceding section, this could be due to the relaxation of the local stress experienced by each defect due to the presence of the other member of the pair, combined with the anharmonicity in the carbon-nitrogen bond. Field and Sherman[17] used the expression

$$\frac{\Delta\nu}{\nu}=(2k)^{-1}\left[\frac{\partial^2 V}{\partial r^2}+3\beta\frac{\partial V}{\partial r}\right] \tag{11}$$

derived by Buckingham[18] for a diatomic molecule, where V is the interaction energy arising from the presence of the environment, β is the bond-anharmonicity coefficient, k is the zero-order force constant, and r is the bond length. The second-derivative term is the additional force constant generated by the lattice, and the first derivative gives the change in the internal force constant caused by the changed equilibrium nuclear spacing. Field and Sherman showed that when a cyanide ion is placed in an alkali halide lattice, the frequency shift due to the repulsive potential between the lattice ions and the impurity atoms is 10 times larger than that from other potentials considered (i.e., Coulombic, polarization, extended quadrupole and Van der Waals potentials), accounting for 85% of the calculated shift. The expected shift between the free-ion case and that of a single ion in various alkali halide lattices was calculated from all potentials and compared with experimentally observed stretching frequency shifts. Reasonable results were obtained.

The repulsive potential between a lattice ion and the isolated cyanide is expressed as

$$(V_{\rm rep})_{\rm ion}=A_{\rm C}e^{-(r_{\rm C}/\rho)}+A_{\rm N}e^{-(r_{\rm N}/\rho)}, \tag{12}$$

where $A_{\rm C}$ and $A_{\rm N}$ are coefficients which depend on the mutual valencies of the carbon or nitrogen and the ion at a given site, respectively. The parameters $r_{\rm C}$ and $r_{\rm N}$ are the respective distances between the carbon and nitrogen atoms and the lattice ion under consideration and ρ is an empirically determined constant. The total potential is obtained by summing this expression for each lattice ion that makes a significant contribution. In the Field-Sherman calculation, the lattice was assumed to be rigid, without distortion with the CN^- ion in place. This must be a good approximation since their results coincide well with experiment. We calculate the displacement of the lattice ions due to the presence of one defect in the pair and reinsert it back into the potential as a perturbation. For our purposes the important displacements are those that provide the mutual stress relief when two defects are near neighbors. Upon inspection of Fig. 13, particularly panel (b), it can be seen that the mutual assistance in outwardly displacing the lattice that we mentioned earlier occurs at the narrow end of the pair. That is, K_A^+ is displaced upward and to the left in the figure by both cyanides. Similarly, $CN_{\rm I}^-$ is assisted in moving K_B^+ upward and to the right by the presence of $CN_{\rm II}^-$.

Shuey and Beyeler[19] evaluated the stress and displacement fields imparted to a cubic lattice by a substitutional elastic dipole as it assumes various orientations. The elastic equations were written in terms of spherical harmonics and approximate solutions were restricted to include harmonics of no higher order than those contained in the exact solution for the isotropic case. They applied their results to the $\langle 100\rangle$ OH^- and $\langle 110\rangle$ O_2^- ions in KCl with reasonable results, although they did question the accuracy for adjacent dipoles. Dick's[5] calculation is another im-

provement in that he expresses the displacements as expansions in the normal-mode (phonon) displacements of the lattice, imposing a modified Debye cutoff to take the discrete lattice into account. This approach should be more appropriate to this application than the spherical harmonic method, yet Beyeler *et al.*[20] studied near-neighbor O_2^- pairs in potassium halides with EPR techniques and externally applied uniaxial stress and found the results to be in agreement with their continuum theory. For the purpose of this paper we use the more manageable expressions for displacements in an isotropic material from Eshelby[21] and Lie and Koehler[22] in order to estimate these displacements, ensuring that the resultant displacements are reasonable in the light of these more sophisticated evaluations. The displacements used are those due to double forces without moment, of magnitude $X_{(d)j}=(v_0\mathbf{C}'\cdot\lambda)_j$, where $v_0=a^3/4$ is the volume of the KCl primitive cell and $\mathbf{C}'$ is the elastic stiffness tensor in the frame of the cyanide impurity. The tensor λ is the intrinsic strain tensor of the CN^- impurity in KCl. Since the impurity is rotationally symmetric about its major axis, in its frame of reference λ is diagonal with two components, λ_1 and λ_2, such that the trace is $\lambda_1+2\lambda_2$. The parameter $\delta\lambda=\lambda_1-\lambda_2$ has been measured ultrasonically by Byer and Sack[23] to be 0.156, and the trace is the fractional change in the volume from the Cl^- ion. Using values taken from x-ray measurements[11,12] we calculate that $\Delta v_0/v_0$ for KCN as opposed to KCl is 0.135, which, in combination with $\delta\lambda$, gives $\lambda_1\simeq\delta\lambda$ and $\lambda_2\simeq 0$. Using these values and the most reasonable choice of elastic constants in the expressions of Lie and Koehler results in a shift of K_B^+ due to CN_I^- in Fig. 13(b) by about 0.04 Å. This is comparable to the results that Dick obtains for ⟨111⟩ impurities in a cubic lattice and with the results of Shuey and Beyeler for ⟨110⟩ O_2^- in KCl,[19] and therefore we take it to be reasonable.

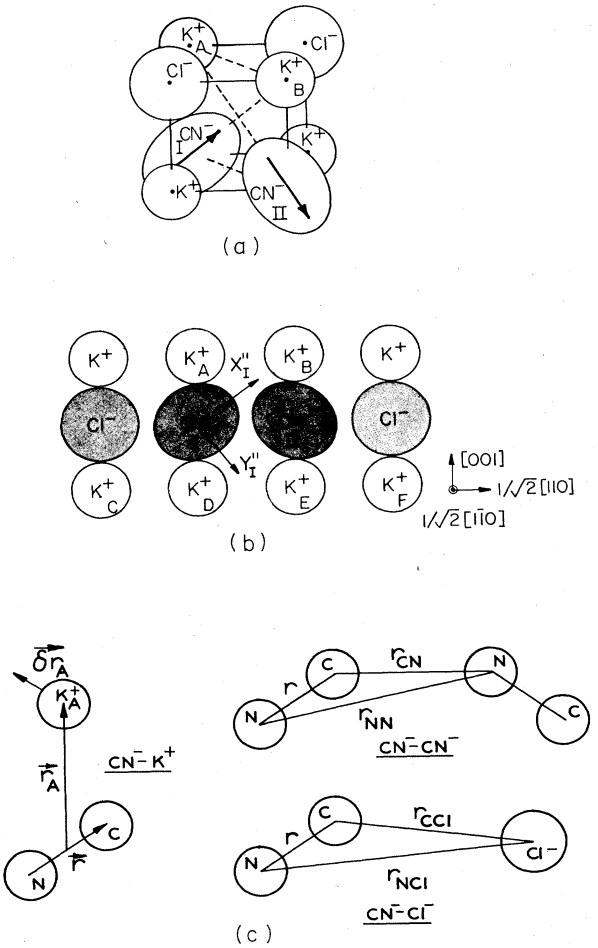

FIG. 13. (a) An isometric rendering of the most probable pair-site configuration. Sizes of cyanides and lattice ions are not to scale. (b) A view of the pair site from the ⟨110⟩ direction of the plane containing the CN^- pair. Ion sites and separations are to scale and the reference frame of the cyanide molecule used in calculations is shown. (c) A representation of the CN^- ion in the (110) plane as a C—N "dumbell" for the calculation of frequency shifts resulting from repulsive interactions with indicated near neighbors.

For the comparative magnitude of the electric interaction and displacement of the lattice ions in the ⟨111⟩ model, the impurity provides a force of singular direction so that the appropriate expressions for such are used from Lie and Koehler. Only the force $\mathbf{F}=-\nabla(e\mathbf{P}\cdot\hat{\mathbf{r}}/\epsilon r^3)$ along the major axis of CN_I^- is considered in displacing K_B^+ in Fig. 13(b). $\mathbf{P}\cdot\hat{\mathbf{r}}$ is 0.07 e Å resulting in a displacement of 0.0004 Å, or a factor of 100 less than by elastic interactions. Thus the electric dipole moment can be neglected in this quantitative analysis and the previous symmetry considerations.

To convert these displacements into frequency shifts, we go back to Eqs. (11) and (12) to evaluate three sources which are judged to have an effect. The frequency shift of CN_I^- in Fig. 13 will be calculated as a result of the presence of CN_{II}^- instead of a Cl^- ion and as a result of the shifts of K_A^+ and K_B^+ due to CN_{II}^-. As in Field and Sherman, the cyanide ion is considered to consist of a carbon and a nitrogen atom which have equal radius and are displaced from each other by $r=1.06$ Å. Also, r_C and r_N in Eq. (12) are expressed as functions of this 1.06-Å separation and the distance to the field atom under consideration from the center of CN_I^- as if the origin were at the center of the impurity. Throughout this calculation, the second-derivative term of Eq. (11) is ignored. Then Eq. (1) becomes

$$(\Delta\nu/\nu)=\left[\frac{3\beta}{2k}\right]\frac{\partial}{\partial r}(A_{C\lambda}e^{-B_{C\lambda}r_{C\lambda}}+A_{N\lambda}e^{-B_{N\lambda}r_{N\lambda}}),$$

where the subscript λ labels the atom or ion under consideration. $A_{C\lambda}$ and $A_{N\lambda}$ are defined by[24]

$$A_{\alpha\lambda}=c_{\alpha\lambda}b_{\alpha\lambda}e^{B_{\alpha\lambda}(r_\alpha+r_\lambda)}, \tag{13}$$

where $c_{\alpha\lambda}$ is a factor calculated by Pauling[13] which gives the dependence of the repulsion on the charges of the ions and r_α and r_λ are the ionic radii. The factors $b_{\alpha\lambda}$ and $B_{\alpha\lambda}$ are empirically determined factors which are determined from the results of Fracassi and Klein[24] and Fumi and Tosi.[25] All values taken from Fumi and Tosi are the average of the values from the two data sets shown in their Table 1.

TABLE II. Parameter values used in the calculation of the downshift of the first sideband due to the pairing model. $\beta=2.16\times10^{8}$ cm^{-1} and $k=1.63\times10^{6}$ ergs/cm^{2}.

Interaction	c	b (10^{12} ergs/molecule)	B (Å^{-1})	r (Å)
CN^--CN^-	0.8	0.264	3.47	1.38
CN-Cl^-	0.775	0.264	$B_{CCl}=3.25$ $B_{NCl}=3.35$	$r_{C,N}=1.38$ $r_{Cl^-}=1.63$
CN-K^+	1.025	0.264	3.19	$r_{C,N}=1.38$ $r_{K^+}=1.51$

We used the value for $A_{\alpha\lambda}$ given in the parentheses in Table 2 of Fracassi and Klein, as these are more consistent with the values of $B_{\alpha\lambda}$ also listed in Table 2 and with the value of $b_{\alpha\lambda}=b=0.264\times10^{-12}$ erg/molecule taken from Fumi and Tosi. This value of b was adopted for all interactions considered here. The radii of the K^+ and Cl^- ions were also assigned the values from Table 1 of Fumi and Tosi. These values are given in our Table II.

Figure 13(c) depicts the spatial arrangement of the atoms in this calculation. Viewing this figure shows that in the CN^--CN^- interaction, the C-N repulsion at the narrow end of the pair is dominant and other repulsion terms will be significantly smaller. For this reason and for simplicity $B_{CN}=3.47$ is used for all terms of this approximate calculation. Using this B_{CN} and the above value for b, we calculate backwards using Eq. (13) from the value of A_{CN} given by Fracassi and Klein to find $r_C=r_N=1.38$ Å. This value of $r_C=r_N$ is also near the average we calculate for r_C and r_N from A_{CC} and A_{NN}. Similarly, calculating backwards from A_{KN}, using the radii for K^+ and Cl^- from Fumi and Tosi, and $r_C=r_N=1.38$ Å both confirms $B_{KC}=3.18$ 1/Å and results in $B_{KN}=3.20$ 1/Å. The average of 3.19 1/Å was used in the calculation of the frequency shift due to the CN^-—K^+ interactions. Finally, we determine the mixed parameters B_{CCl} and B_{NCl} using the approximation

$$B_{\alpha\lambda}=\frac{B_{\alpha\alpha}+B_{\lambda\lambda}}{2}$$

two times in conjunction, with the value of B_{KCl} taken from Fumi and Tosi and B_{CC} and B_{NN} from Fracassi and Klein. These values are also shown in Table II as well as the values of β and k occurring in Eq. (11).

The net shift is the expressed as

$$\Delta\nu_{net}=\left[\left[\frac{\Delta\nu}{\nu}\right]_{CN^-\text{-}CN^-}-\left[\frac{\Delta\nu}{\nu}\right]_{CN^-\text{-}Cl^-}+\delta\left[\frac{\Delta\nu}{\nu}\right]_{CN^-\text{-}K^+}\right](2087\ \text{cm}^{-1})\ .$$

We evaluated this for three different values of the angle θ between the CN^- major axes and the [110] axis connecting them. We also made the calculation for two different values of the CN^--CN^- separation d.[26] We have not calculated the energy of the pair to determine optimum values of θ and d, but it appears reasonable that the cyanides would roll away from ⟨111⟩ alignment, slightly toward a parallel alignment, and their centers of mass would separate somewhat, so that $d>\sqrt{2}a$. (Beyeler[9] pointed out that the observed structure of his high-resolution ir data could be explained by a number of combinations of the fourth- and sixth-order spherical harmonics of cubic symmetry, leading him to conclude that the defect-lattice interaction potential is appreciably deformable by externally applied stress.) The results are given in Table III.

This calculation was also performed on the ⟨111⟩ parallel configuration of Fig. 12. The result and total frequency change was a 1-cm^{-1} downshift, as opposed to 0.7 for the ⟨111⟩ "nodding" configuration. Since these values are comparable, they do not indicate either configuration as energetically preferred. Although electric di-

TABLE III. Calculated frequency shifts based on the ⟨111⟩ "nodding" pair model.

Type of frequency shift	Calculated shift[a] $d=\sqrt{2}a=4.44$ Å $\theta=\cos^{-1}(\frac{2}{3})^{1/2}=35.26°$	$\theta=40°$	$\theta=45°$	$d=4.5$ Å $\theta=45°$
$(\Delta\nu/\nu)_{CN^-\text{-}CN^-}$	0.355	0.270	0.201	0.142
$(\Delta\nu/\nu)_{CN^-\text{-}Cl^-}$	0.216	0.169	0.133	0.097
$(\delta(\Delta\nu/\nu)_{CN^-\text{-}K^+}$	−0.458	−0.602	−0.802	−0.802
$(\Delta\nu/\nu)_{net}$	−0.319	−0.501	−0.734	−0.752
$(\Delta\nu_{net}$ (cm^{-1})[b]	−0.7	−1.0	−1.5	−1.6

[a]All $(\Delta\nu/\nu)$'s are to be multiplied by 10^{-3}.

[b]$\Delta\nu_{net}=[(\Delta\nu/\nu)_{CN^-\text{-}CN^-}-(\Delta\nu/\nu)_{CN^-\text{-}Cl^-}+\delta(\Delta\nu/\nu)_{CN^-\text{-}K^+}](2087\ \text{cm}^{-1})$.

pole coupling is present in this alignment, the odd-symmetry mode would be Raman inactive due to the inversion symmetry and therefore unobserved. The "nodding" configuration provides the cyanide ions in the pair the freedom to realign away from the true ⟨111⟩ directions in order to lower their total energy. In the parallel case they are in the lowest-energy alignment and any realignment only raises the total energy. The "nodding" case may be the preferred configuration in view of this, because the displacement of the near-neighborhood ions of one cyanide in the pair by the other cyanide provides this degree of freedom.

On the basis of these results, we consider the second sideband to be due to triplets of cyanides, yet only triplets such that any one of the defects is near neighbor to both of the other two, as in Fig. 14. In these configurations two cyanides displace the lattice ions that are nearest to the third. We then expect a frequency downshift approximately twice that of the first sideband because we have twice the displacement for the nearest K^+ ions in these configurations than for the pair. This agrees with the separation between the sidebands and the main bands observed in the spectra.

B. Relative sideband intensities

A triplet consisting of a string of impurities in a row along a ⟨110⟩ direction would not give this mutual assistance and the resulting frequency shift. In fact, this configuration will behave more like a pair than a triplet. This picture is corroborated by the integrated intensities of the three separate peaks. For a given cyanide in a sample of cyanide concentration x $(0 \leq x \leq 1)$, the probability of having a cyanide near neighbor is given by a binomial distribution. Since all near-neighbor positions are in ⟨110⟩ directions, there are 12 candidate positions, so that for a given number of cyanide near neighbors n, the probability P_n is given by

$$P_n = \frac{12!}{n!(12-n)!} x^n (1-x)^{12-n} . \tag{14}$$

Then the probability for no, one, and two near neighbors is

$$P_0 = (1-x)^{12}, \quad P_1 = 12x(1-x)^{11}, \quad P_2 = 66x^2(1-x)^{10} .$$

The integrated intensities are not expected to be proportional to these probabilities, because an impurity with two nearest neighbors can be pairlike in behavior and in frequency shift. For any given cyanide with one nearest-neighbor cyanide, only four of the remaining eleven possible sites provide a situation wherein all three cyanides are all nearest neighbors to each other. Thus we expect

$$\frac{P_1'}{P_0} = \frac{\int_{1SB} I\, d\omega}{\int_{MB} I\, d\omega} = \frac{P_1 + \frac{7}{11} P_2}{P_0} ,$$

$$\frac{P_2'}{P_0} = \frac{\int_{2SB} I\, d\omega}{\int_{MB} I\, d\omega} = \frac{4P_2}{11P_0} .$$

Table IV shows the good agreement between the calculated and experimental results.

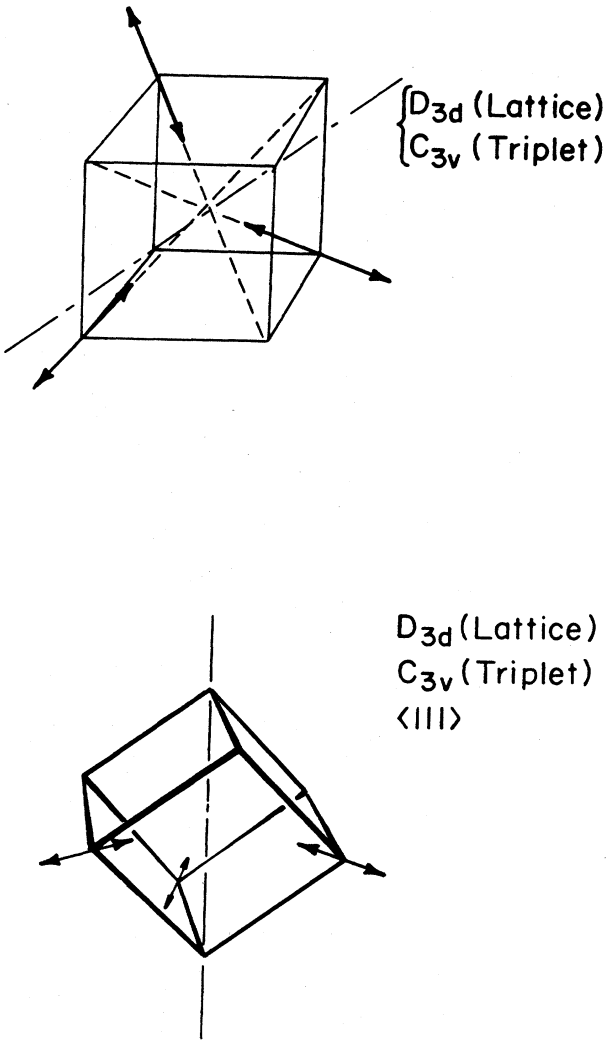

FIG. 14. Two different representations of the triplet indicated by the second sideband.

The small peaks between the sidebands (SB's) and above the main band (MB), as seen in Figs. 1, 3, and 5, might possibly be explained by this type of consideration as well. Although we counted the $\frac{7}{11} P_2$ as being part of the first sideband, and included the extra structure intensities as part of the integrated intensity, most likely these triplets or longer chains that act like pairs to zeroth order do not actually respond as true pairs. For example, in a triplet, because of coupling between the different cyanides that are not near neighbors to each other, the frequency shift due to strain relaxation is probably greater than that in a pure doublet, but less than that of the triplet in which every defect is near neighbor to each of the others. A multiplicity of observed peaks occurs because there are a number of possible triplet and higher-order configurations which exhibit pairlike behavior. All shifts are to lower frequency because the defects in the multiplet act cooperatively to reduce the local strain energy which then reduces their stretching frequency. This then suggests a somewhat negatively skewed structure of these unresolved

TABLE IV. Calculated and measured ratios of the sideband and main-band integrated intensities. I_{1SB} is the integrated intensity of the first sideband, I_{2SB} is the integrated intensity of the second sideband, and I_{MB} is that of the main band.

Sample concentration (mole fraction)	Integrated intensity ratios	Calculated results	Empirical results ($\pm\sigma$)
6.05%	$P_1'/P_0=I_{1SB}/I_{MB}$	0.947	0.98±0.04
	$P_2'/P_0=I_{2SB}/I_{MB}$	0.100	0.094±0.007
	$P_1'/P_0=I_{1SB}/I_{MB}$	1.36	1.44±0.09
8.15%	$P_2'/P_0=I_{2SB}/I_{MB}$	0.182	0.19±0.02
	$P_1'/P_0=I_{1SB}/I_{MB}$	2.12	2.09±0.07
11.1%	$P_2'/P_0=I_{2SB}/I_{MB}$	0.37	0.40±0.02

peaks that combine to comprise the sideband. As temperture is increased, these unresolved peaks broaden thermally to form one continuous, inhomogeneous, Poisson-shaped band, as we described in discussing the data toward the end of the Results section.

A plausible explanation for the narrow structure above the main band is more difficult to provide. The peak is present in the 8% sample in all data of any symmetry taken below 50 K. At 30 K and below the peak has about one-tenth the intensity of the main band in the A_{1g} spectra. Above 37 K this reduces to about one-twentieth the intensity (Fig. 3). The 6% sample has it only from 30 to 54 K and at about one-twentieth the intensity of the main band. The 11% sample shows it below 24 K and always about 5% as intense as the main band. The peak is consistently about 0.8 cm^{-1} higher than the main band. The presence of the peak suggests that these CN^- molecules have assumed an orientation of lower total energy but one of higher stress along the C—N bond. This cannot be due to clustering of CN^- molecules into areas of pure KCN in the samples. Durand and Lüty have shown that the stretching frequency of CN^- in KCN is lower than that of isolated CN^- ions in KCl.[1] It could be, for example, due to CN^- molecules that are near neighbors to OCN^-, which has a higher intrinsic dipole moment than CN^- and is always present to some extent in these KCl:CN^- crystals. The fact that the peak always loses intensity without shifting position implies that the high-stress alignment is maintained, while the state in which the CN^- molecules have lower energy depopulates. Our data are not sufficient to do any more than speculate regarding this feature.

C. Symmetry splitting of the first sideband

We now evaluate the magnitude of the Davydov splitting from the model. The energy of interaction of two electric dipoles is given by Eq. (1) with

$$W_{12}=\frac{-\frac{5}{3}P_1P_2}{\epsilon(\sqrt{2}a)^3} .$$

For the dynamical interaction we make the replacement

$$P_{1,2}\rightarrow\frac{dP}{dr}\delta r_{1,2} ,$$

and $\epsilon=\epsilon_\infty$, and find an interaction energy given by

$$\omega_{12}=\kappa\delta r_1\delta r_2 ,$$

with

$$\kappa=\frac{-\frac{5}{3}(dP/dr)^2}{\epsilon_\infty(\sqrt{2}a)^3} .$$

The solutions to the coupled equations of motion give a splitting of

$$\Delta\omega=\left[\frac{\kappa}{\mu\omega_0^2}\right]\omega_0 ,$$

where μ is the reduced mass of a CN^- molecule. The sign of the interaction in the coupled equations results in the antisymmetric mode having the higher frequency, as we observed. To evaluate $\Delta\omega$, dP/dr can be obtained from the oscillator strength f of the CN^- stretching band via

$$(1/e)\frac{dP}{dr}=\sqrt{3f} ,$$

where f is obtained from "Smakula's Equation."[27–29] Using the data of Beyler,[9,30] we have

$$\frac{1}{e}\frac{dP}{dr}=0.3 ,$$

where e is the electron charge. This results in a splitting of

$$\Delta\omega=0.24\ cm^{-1} .$$

Another interaction mechanism that would couple the stretching oscillations of the two defects is the repulsive force between the electron shells on the narrow end of the nodding pair. The potential of the interaction, similar to Eq. (12), is given by

$$V_{rep}=V_0e^{-Bd}\exp\left[\frac{B}{2}(2r+\delta r_1+\delta r_2)\left[\frac{2}{\sqrt{6}}\right]\right] , \quad (15)$$

where $d=\sqrt{2}a$ is the separation between the cyanides, r represents the C-N separation, and the δr_i are the stretching amplitudes. The factor of $\sqrt{6}$ is included since they lean toward one another along $\langle 111 \rangle$ directions and that of $\frac{1}{2}$ is present since d is the separation at the middle of the cyanides. Reducing this to first order leaves

$$V_{\text{rep}}=\frac{6\gamma}{B^2}\left[1+\frac{B\delta r_1}{\sqrt{6}}\right]\left[1+\frac{B\delta r_2}{\sqrt{6}}\right],$$

where

$$\gamma=V_0(e^{-B[d_0-(2r/\sqrt{6})]})B^2/6 .$$

Then, again, for the force experienced by CN_I^-,

$$(F_{\text{rep}})_I=\frac{-\delta V_{\text{rep}}}{\partial r_1}=-\gamma\delta r_2+c , \tag{16}$$

where c is a constant resulting from the differentiation which does not affect the stretching oscillations. This coupling results in a splitting expressed as:

$$(\Delta\omega)_{\text{rep}}=(\omega_+-\omega_-)_{\text{rep}}=\left[\frac{\gamma}{\mu\omega_0^2}\right]\omega_0 . \tag{17}$$

To evaluate γ, from Fracassi and Klein,[21]

$$V_0=c_{ij}be^{+B(r_c+r_n)} . \tag{18}$$

Here, cij is a factor calculated following Pauling's method[13] to be 0.8, b is 0.264×10^{-12} erg, and $B=3.47$ l/Å as before for the cyanide-cyanide direct interaction, and r_C and r_N are the radii of carbon and nitrogen, respectively, in the CN^- molecule, both approximated to be 1.38 Å.[17] Then,

$$(\omega_+-\omega_-)_{\text{rep}}=0.3\ \text{cm}^{-1} .$$

In this case, the determination of the new basis vectors results in the symmetric mode having the higher frequency because the interaction is repulsive, rather than attractive, as is the electric-dipole—dipole interaction.

Although the electric interaction gives the correct magnitude and the correct symmetry of the higher-frequency mode, the repulsive interaction is comparable to it in magnitude. Yet, the repulsive interaction results in the even-symmetry mode having the higher frequency, contrary to what is observed in the data. The splitting of this first sideband disappears in the temperature interval from 40 to 50 K even though the second sideband shows little change in overall structure or relative position at these temperatures. This implies that the pair maintains its stress-relieving alignment while the state responsible for the splitting depopulates. If the splitting is a result of the repulsive interaction, it is not clear why the splitting does not remain as long as the sideband remains. The dipole interaction depends upon the head-to-tail alignment of the cyanides in the pair. The difference in energy between the two possible alignments of CN_I^- while CN_{II}^- remains fixed is twice the interaction energy in Eq. (2), or

$$\Delta E=2\delta W_{12}=\frac{10}{3}\frac{P^2}{\epsilon(\sqrt{2}a)^3} . \tag{19}$$

Converting P into egs units and using $\epsilon=\epsilon_0$ (both P and ϵ_0 are taken from Holuj and Bridges[31] for consistency between the two values) to evaluate this term shows ΔE to be 14 K. The population of the aligned and antialigned states can be calculated using Boltzmann factors. Now if we ask for a temperature for which the depopulation has begun is not yet completed, then we can say that the antialigned state has about twice the population as the aligned state, resulting in

$$\delta E/k_BT=\Delta E/2k_BT\cong\tfrac{1}{2}\ln2=0.35 . \tag{20}$$

Then, T is $\Delta E/k_B(0.70)$, or 20 K. This is within a factor of 2 of what the data depict. The conclusion is that the electric dipole interaction provides a simple reason for the disappearance of the splitting, whereas the repulsive interaction does not.

In the discussion of the first sideband splitting, it was shown in Table III that the separation of this peak from the main band increases if the impurities in the pair tip away as expected from the $\langle 111 \rangle$ alignment and experience an outward shift of their centers of mass. If we apply the appropriate θ dependence to γ in Eq. (17), we have

$$\gamma=\left[\frac{B\cos\theta}{2}\right]^2V_0e^{-B(d-r\cos\theta)} , \tag{21}$$

and then increasing θ and d to $\theta=40°, d=\sqrt{2}a$; $\theta=45°, d=\sqrt{2}a$; and $\theta=45°, d=4.5$ Å, just as in Table III, results in $(\Delta\omega)_{\text{rep}}=0.2$, 0.15, and 0.1 cm^{-1}, respectively, while $(\Delta\omega)_{\text{elec}}$ stays around 0.2 cm^{-1}. This is sufficient to provide the observed splitting magnitude with the observed symmetry and temperature response.

D. Motional narrowing

Finally, we discuss the motional narrowing observed in the main bands (Fig. 7). Narrowing of this type is an indication that a peak is made up of a large number of discrete states with lifetimes at higher temperatures which are short compared with the reciprocal of the frequency difference between the states.[32] Callender and Pershan[7] reported the main-band width to be $\lesssim 0.4$ cm^{-1} below 100 K for 0.5% CN. This implies that the 1-cm^{-1} width we observe at 4 K must be due to the order of magnitude higher concentrations. De Yoreo *et al.*[33] and Moy *et al.*[34] report that the thermal-conductivity decline and the heat-capacity increase in going from 0.0% to 0.1% KCN in KBr below 10 K are reversed for higher concentrations. This would indicate that the presence of interactions between the impurities hinders the tunneling responsible for the initial effects. The increased low-temperature width that we observe corroborates their conclusions that in the higher concentrations all but a small fraction of the CN^- ions will be frozen in at low temperatures. The resulting distribution of stresses results in a corresponding distribution of stretching frequencies, as was previously discussed, to account for the main-band width. As the temperature increases to 100 K, our data indicate that the CN^- ions collectively and gradually "unfreeze," since we did not observe any sudden change in the main-band width with varying temperatures at these concentrations.

The average distance between the cyanides in the 6%, 8%, and 11% samples is 10.1, 9.1, and 8.2 Å, respectively. These distances are approximately those of next-nearest-neighbors for CN^- in KCl, and the probablity is that there are more than two cyanide ions in this shell. As shown earlier, a shift of the stretching frequency of CN_I^- in Fig. 13(b) is predominantly the result of the spatial shift of K_A^+ or its equivalent directly below CN_I^-. It is highly likely that the number of impurities in this shell can have configurations at low temperature which result in a relative displacement of K_A^+ with respect to CN_I^- on the order of the ± 0.01 to 0.02 Å required to account for the 1-cm^{-1} width that we observe below 10 K. The distribution is attributed to the distribution in the number, location, and population of possible configurations of the non-near-neighbor CN^- ions. This distribution of strain on isolated cyanides throughout the crystal may not be centered about zero, but may result in an upward shift by as much as 0.5 cm^{-1} and still remain within the uncertainty of the measurement of the position of the main band. This could account for some of the separation between the main band and the first sideband.

At 100 K, classical reorientation occurs within a relaxation time determined by the Arrhenius relation

$$\tau_{\text{reor}}=\tau_{\text{libr}}e^{V_0/k_BT}, \tag{22}$$

with τ_{libr} being the period of the librational oscillation and V_0 the well depth. In the case of CN^- in KCl, V_0 is about 45 cm^{-1} or 64 K,[7,9] and τ_{libr} $(=2\pi/\omega_{\text{libr}})$ is $2\pi/16$ cm^{-1} or 2 ps.[2,7] This results in τ_{reor} being about 1 ps at 100 K. In this temperature regime, the system should be in the region of $(\tau_{\text{reor}}\Delta\omega)\ll 1$. If $\Delta\omega$ is taken to be the above-mentioned 0.8 cm^{-1}, then $\tau_{\text{reor}}\Delta\omega$ is 0.16, which satisfies this condition. We can conclude then, that at 100 K all the field impurities are rotating relatively rapidly so that to the single CN^- in question they appear as spheres of volume equal to that of the cyanide ellipsoid. The intrinsic strain tensor for this sphere has the relationship

$$\frac{\Delta v_0}{v_0}=\text{Tr}\lambda_{\text{sph}}=0.149 \text{ such that } \lambda_{\text{sph}}=\left[\frac{0.135}{3}\right]\overleftrightarrow{I}.$$

The displacement of ions due to the presence of a cyanide ion is directly proportional to the intrinsic strain tensor of the impurity. Since this also involves a spherical point source rather than an axial one, calculations indicate a factor of 2 or 3 reduction in the larger displacements caused by rotationally trapped ions. Additional narrowing arises from the rotation of the cyanide under consideration itself. This then is a plausible mechanism by which to account for the observed narrowing of the main-band by a factor of 3 from the low-temperature value to that at a temperature where the cyanides are essentially freely rotating.[35] From this picture, the narrowing should continue at still higher temperatures, but in this 100-K temperature region the width due to this strain interaction may become dominated by the width due to lattice viscosity or T^7 phonon collision broadening.[36] The resulting minimum width should depend on concentration since the amount of motional narrowing depends on frequency shifts due to rotating cyanides at the average, concentration-dependent, intercyanide separation.

VI. COMMENTS AND CONCLUSIONS

The values of some parameters resulting from the least-squares computer fits vary among the different concentrations. According to our model, the amount of the Davydov splitting of the first sideband should not be different for $x=0.06$ than for $x=0.08$ or 0.11 (Fig. 11). Neither should the overall downshift of the stretching frequency of paired cyanides change with concentration. This could be an artifact of the methods we used in fitting the data for peak position. The line shapes of the individual bands are increasingly negatively skewed with increasing concentration. Attempting to fit them with the same symmetric functions could result in different peak positions due to the different line shapes for $x=0.06$, 0.08, or 0.11. However, this would not diminish the validity of the A_{1g} to T_{2g} Davydov splitting for a given concentration since the A_{1g} and T_{2g} spectra for a given x are quite similar in shape.

There is also a change in the average lattice constant with varying x. This would not explain the variation in both of these splitting values since the variation is large (approximately 40% as seen in Fig. 11 and Table I for x between 0.06 and 0.11), yet it does explain the lowered position of the A_{1g} main bands with increasing x as seen in Figs. 8–10. At 100 K, where the minimum of the A_{1g} main-band width occurs, we see main-band positions of 2087.5, 2087.0, and 2086.5 cm^{-1} for $x=0.06$, 0.08, and 0.11, respectively. At this temperature, where a given CN^- experiences the average field of randomly distributed spheres (due to rapid hindered rotation of the other CN^- ions), we would expect only increasing stretching frequencies with increasing higher average stress, which would accompany higher concentration. A possible explanation is that the lattice constant is increasing rapidly enough with concentration to result in decreasing average stress as x increases. In order to show the plausibility of this, we present the following line of reasoning. Callender and Pershan[7] measured the stretching frequency at low temperature of low-concentration KCN in KCl to be 2087.1 and 2077.5 cm^{-1} in KBr. If we assume that the lattice constant (a) of the 6% and 11% solid solutions of KCN and KCl can be obtained by linear interpolation between 6.28 and 6.55 Å, and that the stretching frequency scales linearly with a, then we note a change in stretching frequency of 1 cm^{-1} (2087.5–2086.5 cm^{-1}) accompanying a 0.014-Å change in a [(6.55%–6.28 Å) $\times$(0.11–0.06)]. This amounts to a 71-cm^{-1}/Å decrease in stretching frequency. Now since KBr has a room-temperature lattice constant of 6.57 Å, from KBr:CN^- to KCl:CN^- we have 9.6-cm^{-1} decrease for a 0.29-Å increase in a or 33 cm^{-1}/Å. Since these are within roughly a factor of 2 of each other, it is reasonable to say that much of the decrease in main-band frequency with increasing concentration is due to the increase in the lattice constant.

In summary, although the electric dipole coupling results in full agreement with the data, coupling via the direct repulsive interaction predicts a comparable splitting

but with the wrong symmetry and temperature dependence. Allowing the cyanide ions to tilt away from one another, deviating from the ⟨111⟩ alignment, reduces the repulsive coupling relative to the electric, but only to the point that the combined splitting agrees with our data. This ⟨111⟩ alignment with the same deviating tilt also provides the best agreement with the observed splitting of the first sideband. The width of the main band and its motional narrowing are explained by the strain interaction of non-near-neighbor cyanides in the lattice.

We presently can think of no other picture than this ⟨111⟩ nodding model of near-neighbor CN^- pairs and triplets in KCl:CN^- to so describe our empirical results. It hangs completely on the assumption that the T_{2g}-to-A_{1g} shift in the position of the second sideband is a Davydov-type splitting. We have analyzed this splitting between the symmetries as due to tunneling of the pair as a whole with the symmetry analysis used in Sec. IV and found that such tunneling does not explain the data.

The work of Beyeler *et al.*[19,20] shows that a pair of O_2^- defects has several different orientational configurations with energy differrences of a few meV. Their predictions of the preferred orientations and associated energies have been verified somewhat by an electron-spin-resonance study. Looking at Figs. 4 and 19 of Beyeler, Bauman, and Känzig for O_2^- in KCl and KBr (probably similar in interaction to CN^- in these hosts, although orienting along ⟨110⟩ directions), the difference between the two orientations of least energy is around 50 K. This would indicate that depopulation of these lowest-energy configurations would have begun significantly before 40 to 50 K. We are suprised in the light of these results that we do not observe the earlier disappearance of the A_{1g}-T_{2g} splitting of the first sideband as well as changes in the shape, intensity, and/or relative position of these sidebands. Yet we observe none of these effects or any other new features in this temperature interval. Perhaps this can be attributed to the ⟨111⟩ alignment of CN^- if it does so align when paired.

The Davydov model predicts the correct downshift of pair and triplet stretching frequencies from that of the isolated defect, based on relatively simple, phenomenlogical calculations. Conversely, it is questionable to use macroscopic elastic coefficients in an isotropic continuum model to obtain the shift of near-neighbor lattice ions as a result of the presence of an elongated subtitutional impurity. The numbers so obtained could be in error by factors of 2 or more. We can only say that we have demonstrated the plausibility of the indicated model, although some inconsistencies remain. It is our hope that a more comprehensive theoretical handling of these and other aspects of this system might eventually be undertaken.

The Raman spectra are sensitive to local stress variations in the lattice and therefore provide a good probe with which to detect an order-disorder phase transition. The behavior of the motional narrowing, however, is not consistent with the sudden onset of long-range ordering in the lattice in the temperature and concentration regions covered by this study. It does indicate a frozen disorder consistent with a distribution of well depths at low temperatures, which gradually unfreezes as 100 K is approached. The form of the variation of the main-band width with temperature is reminiscent of that of the TA-phonon frequency as measured by ultrasonic,[37] Brillouin light scattering,[38] and neutron scattering.[39] The measured parameter starts at some finite width at low temperature, falls to a significant fraction of that original value, and finally returns to approximately that value as room temperature is approached. The minimum occurs at a temperature at which the system is in some sense the "softest." The characteristic frequency of this Raman-observed motional narrowing is about 1 cm^{-1} or 30 GHz. If in Fig. 7 we extend a line which is a tangent to the plot of the measured width versus temperature at $T=0$ down to where it intersects the zero-width axis, then we have a representative T_f for this probe of around 80 K for the three concentrations. This frequency-versus-T_f coordinate pair roughly falls on the 10 decade curves of Loidl *et al.*[37] and Bhattacharya *et al.*,[40] thus implying that the same relaxation phenomenon is operable. In a more recent article by Loidl *et al.*,[41] the conclusion is made that below T_f interactions gradually dominate thermal activation, leading to the blocking of CN^- ions into growing clusters of pairs, triplets, etc. If this is true, our data seem to indicate that nearest neighbors are not involved, but rather this effect involves the longer-ranged interactions.

ACKNOWLEDGMENTS

We thank M. W. Klein and B. Fischer for several stimulating discussions on the theory of order-disorder phase transitions and their possible occurrence in these materials, and Clare Yu for suggestions regarding interpretation. This research was sponsored by the National Science Foundation (NSF) under Grants No. DMR-79-02780 and No. DMR-82-03523, and benefited from institutional support through NSF Materials Research Laboratory Grant No. NSF-DMR-80-20250.

*Present address: The Timken Company, Research Division, 1835 Dueber Avenue Southwest, Canton, Ohio 44706.

[1]D. Durand and F. Lüty, Ferroelectrics **16**, 205 (1977).
[2]D. Durand and F. Lüty, Phys. Status Solidi B **81**, 443 (1977).
[3]M. W. Klein, B. Fischer, A. C. Anderson, and P. J. Anthony, Phys. Rev. B **18**, 5887 (1978).
[4]B. Fisher and M. W. Klein, Phys. Rev. Lett. **43**, 289 (1979).
[5]B. G. Dick, Phys. Rev. B **24**, 2127 (1981).
[6]W. Hayes and R. London, *Scattering of Light by Crystals* (Wiley, New York, 1978).
[7]R. Callender and P. S. Pershan, Phys. Rev. A **2**, 672 (1970).
[8]F. Lüty, Phys. Rev. B **10**, 3677 (1974).
[9]H. U. Beyeler, Phys. Rev. B **11**, 3078 (1975).
[10]D. Durand, L. C. S. DoCarmo, A. Anderson, and F. Lüty, Phys. Rev. B **22**, 4005 (1980).
[11]R. G. Wyckoff, *Crystal Structures,* 2nd ed. (Interscience, New York, 1963).
[12]J. M. Bijvoet and J. A. Lely, Rec. Trav. Chem. **59**, 908 (1940).

[13]L. Pauling, Z. Kristallogr. **67**, 377 (1928).
[14]H. S. Sack and M. C. Moriarty, Solid State Commun. **3**, 93 (1965).
[15]A. Lakatos and H. S. Sack, Solid State Commun. **4**, 315 (1965).
[16]M. Julian and F. Lüty, Ferroelectrics **16**, 201 (1977).
[17]G. R. Field and W. F. Sherman, J. Chem. Phys. **47**, 2378 (1967).
[18]A. D. Buckingham, Proc. R. Soc. London, Ser. A **248**, 169 (1958).
[19]R. T. Shuey and H. U. Beyeler, J. Appl. Math. Phys. **19**, 278 (1968).
[20]H. U. Beyeler, R. Baumann, and W. Känzig, Phys. Kondens. Mater. **11**, 286 (1970).
[21]J. D. Eshelby, in *Solid State Physics*, edited by F. Seitz and D. Turnbull (Academic, New York, 1956), Vol. 3, p. 79.
[22]K. C. Lie and J. S. Koehler, Adv. Phys. **17**, 421 (1978).
[23]N. E. Byer and H. S. Sack, Phys. Status Solidi **30**, 579 (1968).
[24]P. F. Fracassi and M. L. Klein, Can. J. Phys. **62**, 725 (1984).
[25]F. G. Fumi and M. P. Tosi, J. Phys. Chem. Solids **25**, 45 (1964).
[26]M. B. Grant, Ph.D. thesis, University of Illinois, 1985 (unpublished).
[27]D. L. Dexter, Phys. Rev. **101**, 48 (1956).
[28]F. Seitz, *Modern Theory of Solids* (McGraw-Hill, New York, 1940), pp. 662—664.
[29]A. Smakula, Z. Phys. **59**, 603 (1930).
[30]Y. Yang, and F. Lüty, Phys. Rev. Lett. **51**, 419 (1983).
[31]F. Holuj and F. Bridges, Phys. Rev. B **20**, 3578 (1979).
[32]R. Kubo, in *Fluctuations, Relaxation and Resonance in Magnetic Systems*, edited by D. ter Haar (Plenum, New York, 1962), pp. 23—68.
[33]J. J. De Yoreo, M. Meissner, R. O. Pohl, J. M. Rowe, J. J. Rush, and S. Susman, Phys. Rev. Lett. **51**, 1050 (1983).
[34]D. Moy, J. N. Dobbs, and A. C. Anderson, Phys. Rev. B **29**, 2160 (1984).
[35]W. D. Seward and V. Narayanamarti, Phys. Rev. **148**, 463 (1966).
[36]R. J. Elliot, W. Hayes, G. D. Jones, H. F. MacDonald, and C. T. Sennett, Proc. R. Soc. London, Ser. A **289**, 1 (1965).
[37]A. Loidl, R. Feile, and K. Knorr, Phys. Rev. Lett. **48**, 1263 (1982).
[38]S. K. Satija and C. H. Wang, Solid State Commun. **28**, 617 (1978).
[39]J. M. Rowe, J. J. Rush, D. G. Hinks, and S. Susman, Phys. Rev. Lett. **43**, 1158 (1979).
[40]S. Bhattacharya, S. R. Nagel, L. Fleishman, and S. Susman, Phys. Rev. Lett. **48**, 1267 (1980).
[41]A. Loidl, R. Feile, K. Knorr, and J. K. Kjems, Phys. Rev. B **29**, 6052 (1984).

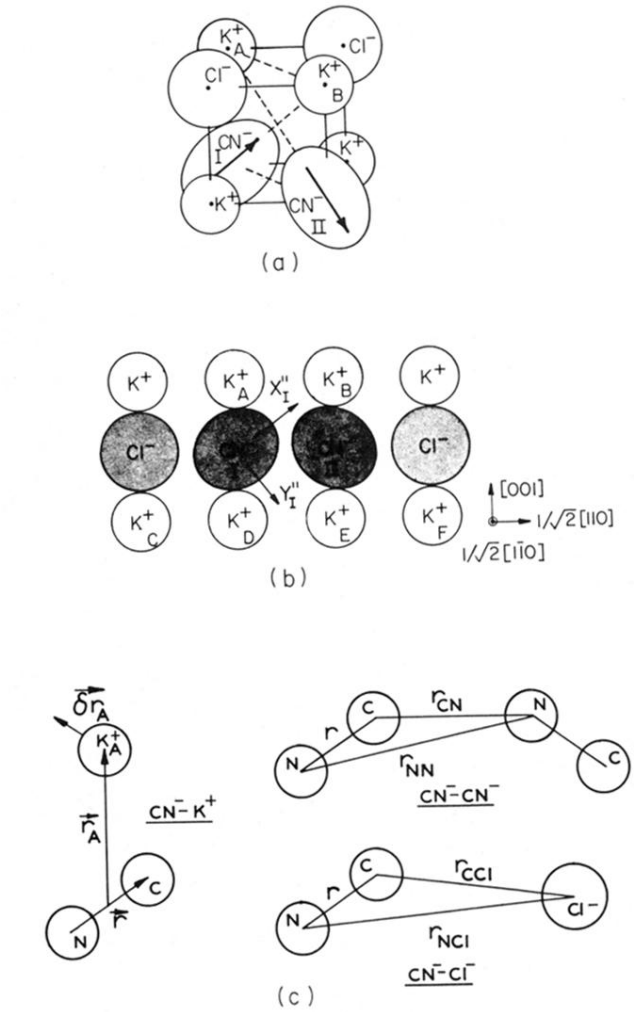

FIG. 13. (a) An isometric rendering of the most probable pair-site configuration. Sizes of cyanides and lattice ions are not to scale. (b) A view of the pair site from the ⟨110⟩ direction of the plane containing the CN^- pair. Ion sites and separations are to scale and the reference frame of the cyanide molecule used in calculations is shown. (c) A representation of the CN^- ion in the (110) plane as a C—N "dumbell" for the calculation of frequency shifts resulting from repulsive interactions with indicated near neighbors.